

Helium recovery by membrane gas separation using Poly(o-acyloxyamide)s (PORAs)

Blanca Díez¹, Purificación Cuadrado¹, Ángel Marcos-Fernández^{1,2}, Pedro Prádanos¹, Alberto Tena^{1,3}, Laura Palacio¹, Ángel E. Lozano^{1,2}, Antonio Hernández^{1*}

¹Smap UA-UVA_CSIC, Universidad de Valladolid, Facultad de Ciencias, Paseo de Belén, 11, 47011 Valladolid, Spain.

²Instituto de Ciencia y Tecnología de Polímeros, CSIC, Juan de la Cierva 3, 28006 Madrid, Spain

³Present address: Helmholtz-Zentrum Geesthacht, Institute of Polymer Research, Max-Planck-Str. 1, 21502 Geesthacht, Germany

* Antonio Hernandez <tonhg@termo.uva.es>

Abstract

Poly-o-acyloxyamides (PORAs) derived from a poly(*ortho*-hydroxyamide) from the 2,2'-Bis(3-amino-4-hydroxyphenyl) hexafluoropropane (APAF) diamine, APAF-POHA, have been synthesized and evaluated as gas separation materials. These polymers were made from poly(o-hydroxyamides) by derivatization of the free OH group with an aliphatic acid dichloride or dianhydride that allowed the introduction of acetyl or pivaloyl groups on their structure. All of them showed low-medium thermal stability due to a degradation of the amide moieties and most of them (those synthesized from isophthaloyl dichloride (IPC), 2,2'-bis(4-carboxyphenyl) hexafluoropropane dichloride (6FC) and 4,4'-dicarboxydiphenylsulfone dichloride (DPSC)) showed good mechanical properties.

These poly-o-acyloxyamides have shown good permselectivities for He/N₂ and He/CH₄ separations and very good permeability-selectivity balance for the He/CO₂ separation. The acetyl PORAs showed better permeability versus selectivity balance than the pivaloyl ones. Moreover, selectivity increased while permeability decreased in the sequence: 6F-APAF → IP-APAF → DPS-APAF

Intersegmental distances, d-spacing values, were shown to decrease along this sequence obtaining a nice correlation between permeability and d-spacing.

Keywords: Gas separation membranes, Helium separation, Poly(o-hydroxyamide)s (POHAs), Poly(o-acyloxyamide)s (PORAs), d-spacing, Free volume fraction.

1 INTRODUCTION

Helium is an inert, low-density gas with a lot of exclusive characteristics which are required for a range of industrial applications and scientific accomplishments. It is the lightest of all gases after hydrogen, it is highly permeable and it has praiseworthy heat transfer properties. It does not become radioactive when exposed to radiation, and remains liquid even near 0K¹. It has been used as a refrigerant in low-temperature devices, as heat transfer agent in nuclear reactors and as a protective and inert atmosphere for purging and pressurizing. It is extensively engaged in shield arc welding technology and leak detection, chromatography, high-field NMR and controlled atmosphere. Other applications are in superconductive, medical, and other advanced technological applications such as space boosters, breathing gas for undersea work, cryogenics, and particularly, applications related to atomic energy¹.

Helium is the second most generously spread element in the cosmos. But, in spite of this, it is very scarce in the earth's rocks where it is in the ppb range, In the atmosphere it reaches only 5.2 ppm per volume². Opportunely, there are accumulations of helium in natural gas reservoirs from where it can be extracted. Helium is in natural gas reservoirs in concentrations ranging from nearly 0.005% to maxima of approximately about 8.0%. Concentrations over 0.3% are considered to be present only in helium-rich natural gas¹.

Helium is one of these materials required for the generation, transmission and storage of renewable energy that often would require reflection on what is sustainability. In the case of helium, its fast depletion from natural gas reservoirs, where it accumulated eras ago, without a reserve for future generations, is not defensible³ and certainly does not conform to the ethical requirements of sustainability. The fusion-energy community habitually defines fusion power as "sustainable" in the ecological sense of the word. But actually helium is required both as a cryogenic gas and as a coolant in fusion plants^{2, 4, 5} and it will continue so unless spectacular advances were done in superconductivity at high or medium temperatures.

1
2
3
4
5 In the last years prices of helium scaled up² going from 50 \$ in 2000 to 160 \$ in 2011
6 per thousand of cubic feet. A helium shortage would cause anarchy in large areas of
7 the global helium-dependent economy, from medical scanners to solders and including
8 optical fibers and LCD screens manufacturers. Moreover, helium is considered a vital
9 element in strategic industries including aerospace and defence^{6, 7}. Due to this
10 strategic character of helium, on October 2, 2013, President Obama in USA signed into
11 law the Helium Stewardship Act of 2013, replacing the Helium Privatization Act of 1996
12 in order to avoid global shortage of helium with significantly higher prices expected for
13 a limited supply⁸. Although USA has 21 % of global helium reserves, it produces 71 % of
14 the world's helium and is the single largest consumer. Helium extracted in Algeria,
15 Poland and Rusia is sold mainly in Europe. Qatar sells its helium almost exclusively in
16 the Asian markets. All these countries own 79 % of the world's reserves although they
17 produce only 29 % of the world's helium⁹.
18
19
20
21
22
23
24
25
26
27

28 Extraction of helium from natural gas typically involves three handling steps⁶; the first
29 step is the removal of impurities including water, carbon dioxide, and hydrogen
30 sulphide from the gas performed by absorption or adsorption and/or other extraction
31 processes. The second stage is the extraction of the high-molecular-weight
32 hydrocarbons. The third step is a cryogenic processing, which removes most of the
33 remaining methane gas. The product is a gas rich in helium containing 50 to 70 percent
34 helium, and including mostly nitrogen, argon, neon, and hydrogen. Final purification of
35 helium is normally done using: (1) activated charcoal absorbers at liquid-nitrogen
36 temperatures and high pressure that can produce 99.9999 percent helium or (2)
37 pressure-swing adsorption (PSA) processes that can yield helium with 99.99 percent
38 purity.
39
40
41
42
43
44
45
46
47
48

49 Membranes, of course, can compete with low temperature sorption and PSA taking
50 advantage of their modularity and easy escalation, low initial investment costs and
51 easy integration in hybrid processes¹⁰. Actually, membrane separation for helium has
52 been tried since the early seventies^{11, 12}. According to Scholes et al., who recently
53 published a survey on the applications of membranes in natural gas processing¹³,
54
55
56
57
58
59
60

1
2
3 direct He/CH₄ separation with membranes affronts a major problem because, due to
4 the very low He concentrations in most of the natural gas reservoirs, very high He
5 selectivities of the order of 1000 are required¹⁰. Although alternatively multi-
6 membrane cascade or hybrid processes have been considered¹³, these processes have
7 considerable energy consumption due to the needed recompression of permeate.
8 Because, as mentioned above, the current procedures separate helium along with
9 nitrogen (plus argon and hydrogen), membrane processes could be developed for the
10 combined removal of N₂ and recovery of He from the raw natural gas by using
11 combined N₂/CH₄ with He/N₂ gas separation membranes without recompression.
12
13
14
15
16
17
18
19

20
21 Herein, we are presenting some new polymeric materials with promising separation
22 performances for gas pairs that includes He. As it will be shown below, these materials
23 have very high permselectivity for the gas couple He/CO₂, notable permselectivity for
24 the He/N₂ pair and good selectivity-permeability compromise for the He/CH₄ couple of
25 gases. As mentioned before, He/N₂ and He/CH₄ separations have a strong importance
26 in helium production processes. On the other hand, He/CO₂ separation also is of great
27 interest if, in this case, helium is taken as a surrogate for H₂^{14, 15}. This assumption of
28 correspondence between He and H₂ is possible because the selectivity for He/H₂ of
29 most of the polymers approaches 1 (going from 0.4 to 1.4)¹⁶. The H₂/CO₂ separation is
30 of great interest in CO₂ capture to avoid or control the “Greenhouse Effect” and to
31 take profit of hydrogen. Efficiently separating CO₂ from H₂ is one of the crucial phases
32 in an environmentally responsible practice during energy production from fossil fuels.
33 Petroleum coke, coal, and also biomass, can be gasified to produce syngas (a mixture
34 of CO and H₂) that can be further reacted with water to produce CO₂ and more H₂. The
35 high temperature, not so high when cogeneration is used, separation of CO₂ to avoid
36 its entrance in the atmosphere and to take profit of H₂ in combustion and/or in fuel
37 cells, is thus a very interesting challenge^{17, 18}.
38
39
40
41
42
43
44
45
46
47
48
49
50
51

52
53 The polymers synthesized here were poly(*ortho*-acyloxyamides) (PORAs) derived from
54 poly(*ortho*-hydroxyamides) obtained from the reaction of 2,2'-Bis(3-amino-4-
55 hydroxyphenyl)hexafluoropropane (APAF) with several aromatic acid dichlorides and
56
57
58
59
60

1
2
3 an ulterior introduction of acetyl or pivaloyl groups on these APAF-POHA by
4 modification reactions.
5
6
7
8
9

10 **2 EXPERIMENTAL**

11 12 13 **2.1 Materials**

14
15
16
17
18 The monomer 2,2'-Bis(3-amino-4-hydroxyphenyl)hexafluoropropane (APAF) was
19 purchased from Apollo Scientific (UK) and purified by vacuum sublimation at 225–230
20 °C.
21
22
23

24
25
26 Terephthaloyl dichloride (TC) and isophthaloyl dichloride (IPC) were bought from
27 Sigma-Aldrich and purified by recrystallization on hexane and a final vacuum
28 sublimation near the melting points of these compounds. The other two aromatic acid
29 dichlorides used, having a SO₂ (DPSC) or a C(CF₃)₃ group (6FC) linking the aromatic
30 rings, were prepared in our laboratory.
31
32
33
34
35
36
37

38 **2.2 Synthesis**

39 40 41 42 **A. Synthesis of Acid Dichlorides**

43
44
45 The acid dichlorides with hinge groups SO₂ and C(CF₃)₃ were synthesized by reaction of
46 the corresponding diacids with 3-fold mol/acid group of thionyl chloride in the
47 presence of some drops of N,N-dimethylformamide, DMF, as catalyst at 60 °C for 6h.
48 The excess of thionyl chloride was distilled off and the remaining solid was purified by
49 recrystallization in toluene and vacuum sublimation at 160-170°C for dichloride having
50 a SO₂ group, and recrystallization in pentane and subsequent purification by vacuum
51 sublimation at 80-90°C for the monomer having a C(CF₃)₃ group.
52
53
54
55
56
57
58
59
60

1
2
3 The scheme of reaction is shown in Figure 1.
4

5
6 *Figure 1. Scheme of the synthesis of the dichlorides from diacids.*
7

8 9 **B. Synthesis of Polymers**

10
11 The general procedure for the synthesis of aromatic poly(*ortho*-hydroxyamide)s,
12 POHAs, consisted in dissolving 5 mmol of the APAF diamine in 5 mL of NMP (N-methyl-
13 2-pyrrolidone) or DMA (dimethylacetamide) at room temperature. Afterwards, the
14 solution was cooled to 0°C and then, the necessary amount of trimethylchlorosilane,
15 TMSCl, (20 mmol) and pyridine (20 mmol) were slowly added. Finally, when the
16 silylation process finished, the temperature of experiment evolved to room
17 temperature and 5 mmol of acid dichloride with 5 mL of solvent were added to the
18 reaction mixture and polycondensation proceeded for 6 hours. The polymer was
19 precipitated and washed with distilled water and dried at 180°C under vacuum to
20 remove occluded solvent.
21
22
23
24
25
26
27
28
29
30
31

32 The preparation of poly(*o*-acyloxyamide)s, PORAs, was carried out experimentally from
33 the poly(*o*-hydroxyamides) by reaction with pivaloyl chloride or acetic anhydride as
34 indicated in the scheme of Figure 2. Modification reaction was essentially carried out
35 by dissolving the corresponding POHA in DMAc and 1.5 mol of reagent/mol of OH
36 group was added in presence of 1.5 mol of pyridine/mol of OH group at room
37 temperature for 5h. After pouring the solution onto water, modified polymer was
38 collected, washed with water for several times and dried at 100 °C under vacuum
39 overnight.
40
41
42
43
44
45
46
47
48

49 ¹H spectra were recorded on Varian AV Agilan 400 spectrometer working at 400MHz
50 using as solvent deuterated dimethylsulfoxide, DMSO-d₆. In order to determine the
51 derivatization degree, samples of 10 mg were used using a relaxation delay higher than
52 7 s at room temperature. The derivatization degree, d_g, was calculated by average of
53 the following ratios: ratio between the OH signal (around 9.5 ppm) and all the
54
55
56
57
58
59
60

1
2
3 aromatic proton signals and as well by determining the ratio between all the aromatic
4 protons and the aliphatic signal associated to the methyl proton of the CH₃-COO
5 moiety (acetyloxy compound) and the methyl protons of the (CH₃)₃C-COO moiety
6 (pivaloyloxy compounds). Both ratios were very alike and the average value was
7 calculated from both measurements. The so obtained derivatization degrees are
8 shown in Table I. It is seen that derivatization for acetyl and pivaloyl polyamides were
9 higher than 74 % and 80%, respectively.
10
11
12
13
14

15
16 *Table I. Derivatization degree of the PORAs obtained from 1H-NMR.*

17
18 The values of inherent viscosity were much lower for the acetyl polymers than those of
19 the pivaloyl polyamides. However, all of them showed ability of being processed on
20 tough films with mechanical properties able to withstand the high pressure employed
21 in gas separation applications.
22
23
24

25
26 *Figure 2. Scheme of poly-o-acyloxyamides PORAs synthesized and studied.*

27
28 Polyamide POHA and PORA films were prepared by casting a filtered 10% (w/v)
29 solution of polymer onto a glass plate and heating at 90°C overnight. Afterwards, the
30 resulting film was thermally treated in an open oven at 80°C for 6 h, and subsequently
31 kept at 180°C under vacuum overnight.
32
33
34
35
36
37

38 **2.3 Membrane Characterization**

39 **A. Attenuated Total Reflectance-Fourier Transform Infra-red Spectroscopy**

40
41
42
43 ATR-FTIR (Attenuated Total Reflectance-Fourier Transform InfraRed spectroscopy)
44 analysis was made at room temperature by using a PerkinElmer Spectrum One infrared
45 spectrometer equipped with an attenuated total reflectance, ATR, accessory. 16 scans
46 taken directly from the films at a resolution of 4 cm⁻¹ were averaged to get the FTIR
47 spectra
48
49
50
51
52
53
54

55 **B. Density and Free Volume Fraction**

1
2
3 The densities, ρ , of the dense membrane films were measured with a Sartorius
4 balance provided with a density kit working according to the Archimedean principle as:
5
6

$$\rho = \rho_0 \frac{W_{air}}{W_{air} - W_{liq}} \quad (1)$$

7
8
9
10
11 where ρ is the density of the film, W_{air} and W_{liq} are the weights of the film in air and in
12 the auxiliary liquid (in this case isooctane)¹⁹, and ρ_0 is the density of the auxiliary liquid.
13
14

15 The fraction of free volume, FFV, can be evaluated by:
16
17

$$FFV = \frac{V - V_0}{V} = \frac{V - 1.3V_w}{V} \quad (2)$$

18
19
20
21
22 where V is the specific volume, $V=1/\rho$, of the polymer at the temperature of interest,
23 and V_0 is the specific volume at 0 K which is estimated as 1.3 times the Van der Waals
24 volume, V_w . Thus the fractional free volume can be estimated from measurements of
25 the polymer density and a calculation of the Van der Waals volume either from group
26 contribution theory of Bondi^{20, 21} or by molecular simulation using an appropriate
27 computational chemistry program.
28
29
30
31
32

33 C. Viscosimetry

34
35
36
37
38
39
40
41
42
43
44
45
46
47
48
49
50
51
52
53
54
55
56
57
58
59
60
Inherent viscosities were measured at 25°C with an Ubbelohde viscometer. Ubbelohde
viscometers are capillary viscometers. Capillary viscometers are, in general, used for
Newtonian, incompressible and wall adherence liquids. The flow inside the capillary is
assumed to be under ideal conditions being laminar, incompressible and stationary.
Moreover, the specificities of the flow at both the entry and the exit of the capillary
are assumed to be negligible and the viscosity to be pressure independent. The time of
transit of polymer solutions in NMP with concentrations below 0.5 g/dL was measured
and the inherent viscosity was obtained.

D. Wide Angle X-ray diffraction

Wide-angle X-ray diffraction (WAXD) patterns were recorded at room temperature in
the reflection mode by using a Bruker D8 Advance diffractometer provided with a PSD
Vantec detector (from Bruker, Madison, Wisconsin). Cu K α radiation ($\lambda = 0.1542$ nm)

1
2
3 was used, operating at 40 kV and 40 mA. The parallel beam optics was adjusted by a
4 parabolic Göbel mirror with horizontal grazing incidence Soller slit of 0.12° and LiF
5 monochromator. The equipment was calibrated with different standards. A step
6 scanning mode was employed for the detector. The diffraction scans were collected
7 within the range of $2\theta = 3\text{--}55^\circ$, with a 2θ step of 0.024° and 0.5 s per step.
8
9

10
11
12 The average intersegmental distances (d-spacing)²², d, can be assessed from the
13 Bragg's law as:
14

$$15 \quad n\lambda = 2d \sin\theta \quad (3)$$

16
17
18 n being the order number, θ the diffraction angle and λ the wave length which
19 corresponds to that of Cu K_α .
20
21

22 23 **E. Differential Scanning Calorimetry**

24
25 DSC (Differential Scanning Calorimetry) experiments were carried out in a Mettler
26 Toledo (DSC 822e) calorimeter equipped with a liquid nitrogen complement. Disc
27 samples cut from the films were sealed in aluminium pans and heated and cooled in
28 order to monitor the thermal response. The heating protocol was as follows: heating
29 from 25°C to the 250 °C at 10°C/min (this final temperature was employed in order to
30 minimize the degradation process); once the target temperature was reached, the
31 sample was cooled at the maximum cooling to 25°C, held at this temperature for 15
32 min and reheated at 10°C/min to detect T_g upto 300 °C.
33
34
35
36
37
38
39

40 41 **F. Thermo-gravimetric Analysis**

42
43 TGA (ThermoGravimetric Analysis) was performed using a Thermal Analysis Q500
44 device. Discs, ranging from 5 to 15 mg in weight, were cut from films and tested. High
45 Resolution (HiRes) mode, with the heating rate automatically adjusted in response to
46 changes in the rate of weight loss, was used with an initial heating rate of 10°C/min
47 under a flux of nitrogen.
48
49
50

51 52 53 54 **G. Strain-stress Analysis**

1
2
3 To complete the study on the physical properties of these polymers, the mechanical
4 properties were measured in tension in an MTS Synergie-200 testing machine
5 equipped with a 100 N load cell. Rectangular test pieces of 5 mm width and 25 mm
6 length were tested. A crosshead velocity of 5 mm/min was used. Strain was measured
7 from crosshead separation and tests were conducted at room temperature
8
9
10

11 12 13 **2.4 Permselectivity**

14
15 The permeability, P , for He, CH₄, N₂, O₂ and CO₂ have been determined by using a
16 permeator with variable pressure (constant volume) operating by the well known *time-*
17 *lag* method. A illustration of the device used has been shown elsewhere²³. The
18 measurements have been carried out at 30 °C and at a pressure of 3 bar.
19
20
21

22
23 According to the *time-lag* operation method, permeability and diffusivity can be
24 obtained directly from the flow rate into the downstream fixed volume when reaching
25 stationary conditions. Solubility, S , can be, in turn, obtained indirectly from measured
26 diffusivities and permeabilities according to $S = P/D$.
27
28
29
30
31
32
33

34 **3 RESULTS AND DISCUSSION**

35 36 37 38 **3.1 Membrane Physicochemical Properties**

39 40 41 42 43 **A. ATR-FTIR Spectroscopy**

44
45 In Figure 3, the ATR-FTIR spectra for the PORAs IP-APAF-Ac and IP-APAF-Pv along with
46 that of the corresponding POHA are shown. Some characteristic for the POHAS can be
47 easily seen:
48
49
50

- 51
52 ▪ **N-H_{st}** from 3500 to 3300 cm⁻¹.
- 53
54 ▪ **O-H_{st}** from 3500 to 3200 cm⁻¹. In polymers this peak is usually wide and often
55 split.
56
57
58
59
60

- $C_{ar}-H_{st}$ in the range 3080-3030 cm^{-1} . This band appears as wide signal caused by the convolution of multiple energy absorptions.
- $C=O_{st}$ symmetric between 1680 and 1670 cm^{-1} .
- $C_{ar}-C_{ar}$ from 1625 to 1575 cm^{-1} and in the 1525-1475 cm^{-1} range
- $N-H \delta$ a weak signal appears in the same zone from 1650 to 1590 cm^{-1} .
- $O-H \delta$ in the vibrational plane, from 1450 to 1200 cm^{-1} .

In turn, PORAs are characterized by having the following absorption bands:

- Disappearance of the OH associated signal from 2500 to 3600 cm^{-1} .
- Appearance of the $\nu_{C=O}$ characteristic of the ester group (both acetyl and pivaloyl) about 1780 cm^{-1} .
- Presence of a band caused by the stretching vibration of the link C-O from the ester that is placed around 1150 cm^{-1} , for the pivaloyl derivatives and around 1200 cm^{-1} for acetyl derivatives.

Figure 3. FTIR spectra of the series of PORAs obtained from the POHA IP-APAF. Also, the corresponding POHA is depicted.

B. Density and FFV

The measured density and evaluated van der Waals specific volume (by the Bondi method) along with the free volume fraction, obtained according to Equations (1) and (2), are shown in Table II. The free volume fractions were bigger for the pivaloyl derivatives than for the acetyl ones according to the bigger size of the pivaloyl group that in addition decreases the rigidity of the polymer chains reducing the T_g as will be mentioned below.

Table II. Density, free volume fraction and inherent viscosity of polymers.

C. Viscosity

1
2
3 The inherent viscosities of the PORAs studied are shown in Table II. As for FFV, there is
4 a clear effect of the higher size of pivaloyl, in this case, increasing the viscosity. It can
5 be settled that for the acetyl PORAs the values of viscosity correspond to medium
6 molecular weight, whereas for PORA-Pv their viscosities (except for the polymer from
7 TC) are high enough to consider that they have high molecular weight. For the sake of
8 comparison the inherent viscosities of the poly(*ortho*-hydroxyamide)s are shown in
9 Table III. As commented above, all the synthesized polymers had enough molecular
10 weight to exhibit film forming properties.
11
12
13
14
15
16

17
18 *Table III. Inherent viscosities of the precursor POHAs.*
19

20 21 22 **D. WAXD** 23

24 Figure 4 shows the diffraction spectra obtained by WAXD for all the PORAs studied. In
25 all cases diffractograms showed no crystallinity peaks, which permit to assert that
26 these structures are amorphous polymers for both the acetyl and pivaloyl PORAs.
27
28
29

30
31 *Figure 4. WAXD analysis of acetyl (a) and pivaloyl (b) PORAs.*
32

33 The corresponding d-spacings appear in Table IV. In amorphous polymers the values of
34 d can be correlated directly with the size of the free volume elements through which
35 gases diffuse^{22, 24}. Note that also, in this case, the bigger size of the pivaloyl group leads
36 to slightly higher intersegmental lengths for the corresponding PORAs.
37
38
39

40
41 *Table IV. WAXD results for the PORAs studied in this work.*
42

43 The values of FFV and d-spacing seem to be both determined by the size of the added
44 group, linked respectively to the total free volume and to the mean size of the
45 individual holes forming the free volume, which could be correlated as it is depicted in
46 Figure 5. It seems clear that, although it could be otherwise, in our case there is an
47 approximately monotonous increase of total free volume fraction for increasing
48 average size of the individual holes.
49
50
51
52

53
54 *Figure 5. Free volume fraction as a function of intersegmental distance.*
55
56
57
58
59
60

Such kind of relationships have been recognized as determined by a spreading apart of the chains with larger d-spacing that would cause an increase in free volume to accommodate a packing as tight as possible²⁴.

E. DSC

The glass transition temperature revealed by differential scanning calorimetry is shown, for the PORAs studied, in Table V. T_g increases in the sequence



for the pivaloyl PORAs. Although the acetyl derivatives showed always higher T_g than the pivaloyl ones a similar tendency is followed. Lower T_g for the pivaloyl samples could be due to a slight disruption of chain rigidity induced by the bulkier pivaloyl groups.

Table V. Thermogravimetric results along with the DSC (T_g) ones for the PORAs studied.

F. Thermogravimetry

The onset temperature for mass loss according to thermogravimetric analysis along with the total carbon residues at 800°C, R_c , and the weight loss from 50 to 300°C, W_L , are shown in Table V. The corresponding graphs for cumulative and differential mass loss are shown in Figure 6 for the DPS-APAF both pivaloyled and acetyled.

Figure 6. TGA analysis for the acetyl (a) and pivaloyl (b) DPS-APAF PORAs.

On analyzing these results, it can be seen that a strong and rapid degradation takes place at temperatures above 250 °C (values for the pivaloyl derivative were slightly higher). The final char yield was low with values lower than 30%. This rapid and relatively medium-temperature weight loss cannot be attributed to a partial formation of polybenzoxazole, which it is observed for ortho-OH polyamides. Details of the degradation mechanism will be commented elsewhere, but it could be commented here that the electron-withdrawing effect of the acyloxy groups lessens the thermal stability of the amide group.

G. Mechanical Properties

1
2
3 An example of a strain-stress curve, in this case, for the IP-APAF-Ac and IP-APAF-Pv are
4 shown in Figure 7. Some characteristic²⁵ parameters are shown on the figure. It is
5 clearly observed that mechanical properties were not very different for the acetyl
6 PORAs respect to the pivaloyl ones, although the later showed higher Young modulus
7 but lower failure strain. It is worth noting that mechanical properties were good except
8 for the case of those made out of the terephthaloyl dichloride that broke at low
9 strains, probably due to a lower polymerization degree. Mechanical properties for
10 acetylated PORAs were high enough despite of the lower molecular weight as
11 indicated by their lower inherent viscosity values.
12
13
14
15
16
17
18
19

20 *Figure 7. Stress-strain curves for APAF-IP-Ac and APAF-IP-Pv polymers.*

21 22 23 24 25 **3.2 Permeability and Selectivity**

26
27 The permeability of helium through the PORAs membranes along with their selectivity
28 towards the gas couples He/N₂ and He/CH₄ are shown in Figure 8. In this figure, the
29 gray symbols correspond to the results used by Robeson in his last revision of his
30 permeability-selectivity upper bound^{26,16}. Moreover, the zones with more
31 accumulation of polymer representative points are here surrounded by gray lines.
32 Note that the points fit well within the accumulation clouds for the He/N₂ couple. For
33 the He/CH₄ pair the situation was slightly better for some results. This is especially true
34 for DPS-APAF-Ac which has an outstanding selectivity although with a moderate
35 permeability. In both cases, the line of closer approximation to the upper bound
36 showed that clearly the acetyl derivatives have better permselectivities than the
37 pivaloyl ones. The best permeability-selectivity compromise was shown by the 6F-
38 APAF-Ac followed by the IP-APAF-Ac and finally by the DPS-APAF-Ac. In this order,
39 permeability decreases while selectivity is almost constant although evidencing a slight
40 decline.
41
42
43
44
45
46
47
48
49
50
51
52

53 *Figure 8. Robeson plot for He/N₂(a) and He/CH₄(b) for all the APAF PORAs studied. Black*
54 *symbols correspond to the acetyl PORAs while white signs correspond to the pivaloyl ones.*

55
56 In Figure 9, permeability and selectivity for the He/CO₂ couple of gases are shown,
57 again in a Robeson's plot. In this case the order of decreasing permeability is the same
58
59
60

1
2
3 as for the other pairs of gases but selectivity increases substantially instead of being
4 almost constant. In this case, a decrease in permeability was accompanied with a sharp
5 increase in selectivity. The DPS-APAF-Ac had a quite high selectivity approaching the
6 1991²⁶ upper bound for the He/CO₂ pair, being one of the polymers placed closest to
7 the upper bound^{16, 27} in the high selectivity region. This polymer was well placed out of
8 the cloud observed for the most frequent polymers for this couple of gases.
9
10
11
12

13
14
15 It is worth mentioning that the original 1991 Robeson's bound, as pointed out by
16 Robeson himself¹⁶ would have been mostly conserved if some perfluorinated polymer
17 data had not been considered from literature. These polymers are placed in the
18 medium to high permeability zones of the plot. Moreover selectivities, as high as 300
19 but having He permeabilities as low as 0.1 Barrer were seen in the 1991 upper-
20 bound¹⁶.
21
22
23
24
25
26
27

28 *Figure 9. Robeson plot for He/CO₂ for all the APAF PORAS studied. Black symbols correspond to*
29 *the acetyl PORAs while white symbols correspond to the pivaloyl ones.*
30

31 It is known²⁸ that diffusivity can be correlated with FFV, according to Fujita's theory²⁹
32 of diffusion, as:
33
34
35

$$36 \quad D = A_D e^{-B / FFV} \quad (4)$$

37
38 with A_D and B constants for a given gas and polymer. These factors are correlated with
39 the size and kinetic velocity of the penetrant, A_D, and the free volume of holes needed
40 for penetrant diffusion, B. Then:
41
42
43
44

$$45 \quad P = S A_D e^{-B / FFV} \quad (5)$$

46
47
48 Equation (5) allows the correlation of FFV with permeability and solubility S. Lee³⁰
49 originally correlated the permeability of various polymers to their specific free volume.
50 Hensema³¹ made an analogous plot including polyimides, polyoxadiazoles and
51 polytriazoles and found different values for A and B. Finally Park and Paul³² proposed a
52
53
54
55
56
57
58
59
60

1
2
3 general correlation based on more than 100 glassy polymers representing a wide
4 variety of structural types.
5
6

7
8 Although this correlation has been proved by us for some commercial polymers³³, it is
9 not perfectly followed for our structures. It seems clear that also free volume
10 distribution and sizes of the narrower necks connecting hole to hole had to be taken
11 into account. Therefore, it is actually possible that smaller total free volumes could
12 include wider necks or throats producing higher diffusivities. In Figure 10 the straight
13 lines correspond to Equation (5). It can be seen that although this correlation is not
14 perfect it is approximately valid for our polymers. Of course, when trying to correlate
15 permeability with FFV according to Eq. (5), the possibility of dealing with different
16 solubility values, S , must be taken into account. Nagel et al.³⁴ analyzed directly
17 diffusivity, thus solubility should not be disturbing, and they determined that Eq. (4)
18 should be followed. Their results showed again a rough accordance with FFV although
19 their FFV values were achieved from positron annihilation lifetime spectroscopy (PALS)
20 and thus they should be more reliable than any based on the group contribution
21 theory used here.
22
23
24
25
26
27
28
29
30
31
32

33 *Figure 10. Permeability to all the gases studied as a function of 1/FFV.*
34

35 Permeability correlated also with other various parameters that characterize chain
36 packing, such as the mean interchain distance (d -spacing deduced from wide-angle X-
37 ray diffraction (WAXD) studies)^{35,36}.
38
39
40
41
42

43 Figure 11 shows the permeability to helium and carbon dioxide along with the
44 selectivity of the He/CO₂ pair as a function of the intersegmental distance, d , obtained
45 from WAXD experiments. It seems clear that permeability increases approximately
46 linearly with d and is higher for the smallest gas (in Figure 11a the molecular size for
47 both gases are shown as stars). The He/CO₂ selectivity increases abruptly when d
48 decreases, which leads to a very high selectivity when d approaches the size of CO₂.
49 The size volumes showed in Figure 11 were taken from literature³⁷⁻⁴⁰ and they were
50 2.58 Å for He, 2.96 Å for H₂ and 3.87 Å for CO₂. The corresponding kinetic diameter, as
51
52
53
54
55
56
57
58
59
60

1
2
3 taken from sorption data on zeolites, were 2.6 Å for He, 2.9 Å for H₂ and 3.3 Å for CO₂
4
5^{38, 41}.

6
7
8
9
10
11
12
13
14
15
16
17
18
19
20
21
22
23
24
25
26
27
28
29
30
31
32
33
34
35
36
37
38
39
40
41
42
43
44
45
46
47
48
49
50
51
52
53
54
55
56
57
58
59
60

Figure 11. Permeability of He and CO₂ (a) and He/CO₂ selectivity (b) as a function of the intersegmental distance (d-spacing). Stars in (a) correspond to the hard sphere molecular diameter of He and CO₂. The hard sphere size of H₂ is also marked as a vertical dash.

The correlation of permeability and structure has been investigated in depth by Hirayama et al.^{42, 43}. They showed that, for several polyimides, the diffusivity versus d-spacing correlation was discrete although this correlation was also poor for the correlation of diffusivity versus 1/FFV. A better but not really complete correlation of permeability with d-spacing and 1/FFV has been found by Bas et al.⁴⁴ for several polyimide membranes as a part of an investigation of the correlation of functional versus several structural parameters.

It has been shown that there is a significant increase of intersegmental spacing of various glassy polymers after an exposure to CO₂⁴⁵ mostly at high pressures, which produces plasticization. This increase of d-spacing leads to the characteristic increments in permeability. It has also been shown that PVC-POEM grafted copolymers increase d-spacing and permeability when the amount of POEM increases⁴⁶. Nagel et al.³⁴ measured higher d-spacing in highly selective polymers (glassy poly(amide imide)s, poly(ester imide)s, and polyimides) with high permeabilities and therefore with elevated FFV.

In summary, more accurate correlations of d-spacing, and of FFV, with permeability seem to be obtained when analogue series of polymers are considered. This result seems to confirm that both d-spacing and FFV are not completely descriptive of the polymer and their transport properties. The solubility and distribution of the size of the holes and of the radii of the throats connecting them should be similar in order to achieve a clear correlation of FFV and d-spacing with permeability.

4 CONCLUSIONS

Medium thermally stable poly(o-acyloxyamide)s (PORAs) have been obtained and their characteristics studied in detail. Thermal and mechanical properties have been studied confirming the good processability of most of them.

These poly(o-acyloxyamide)s have been shown to have good gas separation properties when Helium is a component of the mixture to be separated, and this finding is especially true for He/CO₂ separations. Attending to the relevance of this separation and also to the similarity of He and H₂ in gas separation, which could be translated to even more significant H₂/CO₂ separation, it could be inferred that this result is quite promising. Excellent results have been obtained for the He/N₂ separation and good permselectivity for the He/CH₄ separation.

The best selectivity-permeability compromises were attained by the acetyl PORAs whereas the pivaloyl ones showed lower gas separation properties. Selectivity increased and permeability decreased in the sequence

6F-APAF -- IP-APAF -- DPS-APAF

The permeability values versus FFV and as well versus d-spacing have been tested obtaining a nice correlation between permeability and intersegmental, d-spacing, distance.

5 ACKNOWLEDGEMENTS

Authors would like to thank the Ministry of Economy and Competitiveness (MINECO) for the financial support of this work within the framework of the Plan Nacional de I+D+I through the research projects MAT2011-25513, MAT2010-20668 and CTQ2012-31076. Also the Spanish "Junta de Castilla y Leon" has contributed through the project VA248U13. Authors also greatly appreciated the help provided by Sara Rodriguez in measuring gas separation properties.

6 REFERENCES

1. Liu, B.-c., Helium conservation and supply and demand projections in the USA. *Energy Economics* **1983**, 5, (1), 58-64.
2. Bradshaw, A. M.; Hamacher, T., Nuclear fusion and the helium supply problem. *Fusion Engineering and Design* **2013**, 88, (9–10), 2694-2697.
3. Cook, E., The Helium Question. *Science* **1979**, 206, (4423), 1141-1147.
4. Nuttall, W. J.; Clarke, R. H.; Glowacki, B. A., Resources: Stop squandering helium. *Nature* **2012**, 485, (7400), 573-575.
5. William J. Nuttall, R. H. C., Bartek Andrzej Glowacki(eds), *The Future of Helium as a Natural Resource*. Routledge: Abingdon/New York, 2012.
6. *The Impact of Selling the Federal Helium Reserve*. The National Academies Press: Washington, 2000.
7. *Selling the nation's helium reserve*. The National Academies Press: Washington, 2010.
8. Interior, U. D. o. Helium. <http://www.blm.gov/nm/st/en/prog/energy/helium.html> (04/12/2014),
9. Garvey, M. D. Up, up and away. Where has all the helium gone? <http://www.blm.gov/nm/st/en/prog/energy/helium.html> (04/12/2014),
10. *Membrane handbook*. Kluwer Academic Publishers: Dordrecht (The Netherlands), 2001.
11. Agrawal, J. P.; Sourirajan, S., Helium separation by cellulose acetate membranes. *Journal of Applied Polymer Science* **1969**, 13, (5), 1065-1068.
12. Gantzel, P. K.; Merten, U., Gas Separations with High-Flux Cellulose Acetate Membranes. *Industrial & Engineering Chemistry Process Design and Development* **1970**, 9, (2), 331-332.
13. Scholes, C. A.; Stevens, G. W.; Kentish, S. E., Membrane gas separation applications in natural gas processing. *Fuel* **2012**, 96, (0), 15-28.
14. Abedini, R.; Nezhadmoghadam, A., APPLICATION OF MEMBRANE IN GAS SEPARATION PROCESSES: ITS SUITABILITY AND MECHANISMS *Petroleum & Coal* **2010**, 52, (2), 69-80.
15. Luebke, D. R.; Pennline, H. W.; Myers, C. R. In *Surface Selective Membranes for Carbon Dioxide Separation* Twenty-Second Annual International Pittsburgh Coal Conference, Pittsburgh 2005; Pittsburgh 2005.
16. Robeson, L. M., The upper bound revisited. *Journal of Membrane Science* **2008**, 320, (1–2), 390-400.
17. Lin, H.; Van Wagner, E.; Freeman, B. D.; Toy, L. G.; Gupta, R. P., Plasticization-Enhanced Hydrogen Purification Using Polymeric Membranes. *Science* **2006**, 311, (5761), 639-642.
18. Myers, C.; Pennline, H.; Luebke, D.; Ilconich, J.; Dixon, J. K.; Maginn, E. J.; Brennecke, J. F., High temperature separation of carbon dioxide/hydrogen mixtures using facilitated supported ionic liquid membranes. *Journal of Membrane Science* **2008**, 322, (1), 28-31.
19. Brandrup, J.; Immergut, E. H.; Grulke, E. A., *Polymer handbook*. 4th ed. ed.; John Wiley & Sons Inc: New York, 1999.
20. Bondi, A., van der Waals Volumes and Radii. *The Journal of Physical Chemistry* **1964**, 68, (3), 441-451.
21. Van Krevelen, D. W., *Properties of Polymers: their Correlation with Chem Structure: their Numerical Estimation and Prediction from Additive Group Contributions*. Elsevier: Amsterdam, The Netherlands, 1990.
22. Klug, H. P.; Alexander, L. E., *X-Ray Diffraction Procedures*. J. Wiley&Sons: New York 1974.
23. Marchese, J.; Anson, M.; Ochoa, N. A.; Prádanos, P.; Palacio, L.; Hernández, A., Morphology and structure of ABS membranes filled with two different activated carbons. *Chemical Engineering Science* **2006**, 61, (16), 5448-5454.

- 1
- 2
- 3 24. Halasa, A. F.; Wathen, G. D.; Hsu, W. L.; Matrana, B. A.; Massie, J. M., Relationship
- 4 between interchain spacing of amorphous polymers and blend miscibility as determined by
- 5 wide-angle X-ray scattering. *Journal of Applied Polymer Science* **1991**, 43, (1), 183-190.
- 6 25. Callister, W. D., *Materials Science and Engineering. An introduction*. Sixth Edition ed.;
- 7 John Wiley & sons Inc.: New York, USA, 2003.
- 8 26. Robeson, L. M., Correlation of separation factor versus permeability for polymeric
- 9 membranes. *Journal of Membrane Science* **1991**, 62, (2), 165-185.
- 10 27. Robeson, L. M.; Burgoyne, W. F.; Langsam, M.; Savoca, A. C.; Tien, C. F., High
- 11 performance polymers for membrane separation. *Polymer* **1994**, 35, (23), 4970-4978.
- 12 28. Matteucci, S.; Yampolskii, Y.; Freeman, B. D.; Pinnau, I., Transport of Gases and Vapors
- 13 in Glassy and Rubbery Polymers. In *Materials Science of Membranes for Gas and Vapor*
- 14 *Separation*, Yampolskii, Y.; Pinnau, I.; Freeman, B. D., Eds. John Wiley & Sons Ltd: Chichester,
- 15 UK, 2006.
- 16 29. Fujita, H., Diffusion in polymer-diluent systems. In *Fortschritte Der Hochpolymeren-*
- 17 *Forschung*, Springer Berlin Heidelberg: 1961; Vol. 3/1, pp 1-47.
- 18 30. Lee, W. M., Selection of barrier materials from molecular structure. *Polymer*
- 19 *Engineering & Science* **1980**, 20, (1), 65-69.
- 20 31. Hensema, E. R. Polyoxadiazole and polytriazole gas separation membranes. Synthesis
- 21 and properties. University of Twente, Twente, The Netherlands, 1991.
- 22 32. Park, J. Y.; Paul, D. R., Correlation and prediction of gas permeability in glassy polymer
- 23 membrane materials via a modified free volume based group contribution method. *Journal of*
- 24 *Membrane Science* **1997**, 125, (1), 23-39.
- 25 33. Recio, R.; Lozano, Á. E.; Prádanos, P.; Marcos, Á.; Tejerina, F.; Hernández, A., Effect of
- 26 fractional free volume and Tg on gas separation through membranes made with different
- 27 glassy polymers. *Journal of Applied Polymer Science* **2008**, 107, (2), 1039-1046.
- 28 34. Nagel, C.; Günther-Schade, K.; Fritsch, D.; Strunskus, T.; Faupel, F., Free Volume and
- 29 Transport Properties in Highly Selective Polymer Membranes. *Macromolecules* **2002**, 35, (6),
- 30 2071-2077.
- 31 35. Charati, S. G.; Houde, A. Y.; Kulkarni, S. S.; Kulkarni, M. G., Transport of gases in
- 32 aromatic polyesters: Correlation with WAXD studies. *Journal of Polymer Science Part B:*
- 33 *Polymer Physics* **1991**, 29, (8), 921-931.
- 34 36. O'brien, K. C.; Koros, W. J.; Husk, G. R., Polyimide materials based on pyromellitic
- 35 dianhydride for the separation of carbon dioxide and methane gas mixtures. *Journal of*
- 36 *Membrane Science* **1988**, 35, (2), 217-230.
- 37 37. Bischoff, B. L.; Judkins, R. R., Development of Inorganic Membranes for Hydrogen
- 38 Separation. In *Inorganic Chemistry: Reactions, Structure and Mechanisms*, Trimm, H. H., Ed.
- 39 CRC Press: 2011.
- 40 38. Breck, D. W., *Zeolite molecular sieves: structure, chemistry and use*. John Wiley & Sons:
- 41 New York, 1974.
- 42 39. de Vos, R. M.; Verweij, H., High-Selectivity, High-Flux Silica Membranes for Gas
- 43 Separation. *Science* **1998**, 279, (5357), 1710-1711.
- 44 40. Jiang, D.-e.; Cooper, V. R.; Dai, S., Porous Graphene as the Ultimate Membrane for Gas
- 45 Separation. *Nano Letters* **2009**, 9, (12), 4019-4024.
- 46 41. Kim, T. H.; Koros, W. J.; Husk, G. R.; O'Brien, K. C., Relationship between gas separation
- 47 properties and chemical structure in a series of aromatic polyimides. *Journal of Membrane*
- 48 *Science* **1988**, 37, (1), 45-62.
- 49 42. Hirayama, Y.; Yoshinaga, T.; Kusuki, Y.; Ninomiya, K.; Sakakibara, T.; Tamari, T., Relation
- 50 of gas permeability with structure of aromatic polyimides I. *Journal of Membrane Science*
- 51 **1996**, 111, (2), 169-182.
- 52 43. Hirayama, Y.; Yoshinaga, T.; Kusuki, Y.; Ninomiya, K.; Sakakibara, T.; Tamari, T., Relation
- 53 of gas permeability with structure of aromatic polyimides II. *Journal of Membrane Science*
- 54 **1996**, 111, (2), 183-192.
- 55
- 56
- 57
- 58
- 59
- 60

- 1
2
3 44. Bas, C.; Mercier, R.; Dauwe, C.; Albérola, N. D., Microstructural parameters controlling
4 gas permeability and permselectivity in polyimide membranes. *Journal of Membrane Science*
5 **2010**, 349, (1–2), 25-34.
6 45. Houde, A. Y.; Kulkarni, S. S.; Kulkarni, M. G., Permeation and plasticization behavior of
7 glassy polymers: a WAXD interpretation. *Journal of Membrane Science* **1992**, 71, (1–2), 117-
8 128.
9 46. Ahn, S. H.; Seo, J. A.; Kim, J. H.; Ko, Y.; Hong, S. U., Synthesis and gas permeation
10 properties of amphiphilic graft copolymer membranes. *Journal of Membrane Science* **2009**,
11 345, (1–2), 128-133.
12
13
14
15
16
17
18
19
20
21
22
23
24
25
26
27
28
29
30
31
32
33
34
35
36
37
38
39
40
41
42
43
44
45
46
47
48
49
50
51
52
53
54
55
56
57
58
59
60

TABLES

Table I. Derivatization degree of the PORAs obtained from $^1\text{H-NMR}$.

Polymer	d_g (%)	Polymer	d_g (%)
IP-APAF-Ac	82	IP-APAF-Pv	81
T-APAF-Ac	79	T-APAF- Pv	91
6F-APAF-Ac	76	6F-APAF- Pv	87
DPS-APAF -Ac	74	DPS-APAF - Pv	80

Table II. Density, free volume fraction and inherent viscosity of polymers.

Polymer	ρ (g/mL)	$V_w(\text{\AA}^3)$	FFV	η_{inh} (dL/g)
IP-APAF-Ac	1.398	442.20	0.166	0.38
T-APAF-Ac	1.396	440.74	0.174	0.30
6F-APAF-Ac	1.422	581.89	0.199	0.46
DPS-APAF-Ac	1.395	544.58	0.178	0.35
Polymer	ρ (g/mL)	$V_w(\text{\AA}^3)$	FFV	η_{inh} (dL/g)
IP-APAF--Pv	1.252	542.53	0.200	0.80
T-APAF -Pv	1.277	542.67	0.183	0.33
6F-APAF -Pv	1.115	680.63	0.335	0.77
DPS-APAF -Pv	1.340	644.28	0.162	0.67

Table III. Inherent viscosities of the precursor POHAs.

Polymer	IP-APAF	T-APAF	6F-APAF	DPS-APAF
η_{inh} (dL/g)	0.79	0.46	0.82	0.56

Table IV. WAXD results for the PORAs studied.

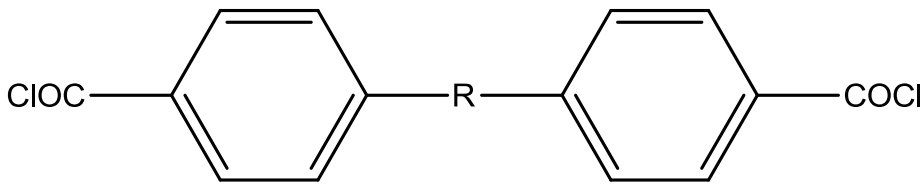
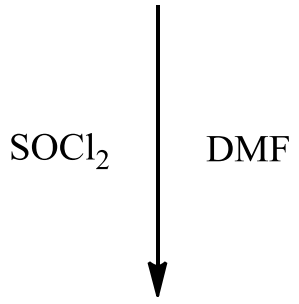
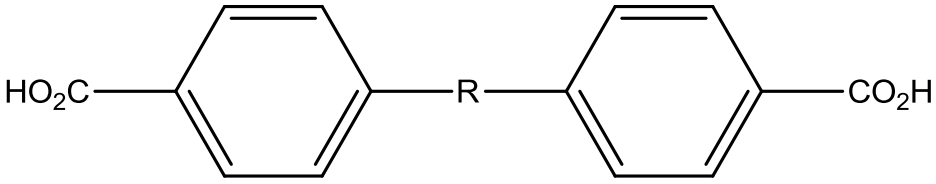
Polymer	2 θ (deg)	d (Å)
IP-APAF-Ac	18.0	4.9
T-APAF-Ac	16.6	5.3
6F-APAF-Ac	16.0	5.5
DPS-APAF-Ac	18.8	4.7
Polymer	2 θ (deg)	d (Å)
IP-APAF-Pv	16.1	5.5
T-APAF -Pv	16.9	5.3
6F-APAF -Pv	15.8	5.6
DPS-APAF -Pv	17.6	5.0

Table V. Thermogravimetric results along with the DSC (T_g) ones for the PORAs studied.

Polymer	Temperature (°C)		% R _c Residue (800°C)	% W _L weight loss (300°C)
	T _o (TGA ONSET)	T _g		
IP-APAF-Ac	243	167	21	27
T-APAF-Ac	259	159	22	26
6F-APAF-Ac	245	196	18	23
DPS-APAF-Ac	271	183	27	24
Polymer	Temperatura (°C)		% R _c (800°C)	% weight loss
	T _{onset}	T _g		
IP-APAF-Pv	258	130	15	38
T-APAF -Pv	257	145	20	35
6F-APAF -Pv	263	153	22	23
DPS-APAF -Pv	269	168	28	24

FIGURE CAPTIONS

- 1
2
3
4
5
6
7
8
9
10
11
12
13
14
15
16
17
18
19
20
21
22
23
24
25
26
27
28
29
30
31
32
33
34
35
36
37
38
39
40
41
42
43
44
45
46
47
48
49
50
51
52
53
54
55
56
57
58
59
60
- Figure 1.** Scheme of the synthesis of the dichlorides from diacids.
- Figure 2.** Scheme of the poly-o-acyloxyamides PORAs synthesized and studied.
- Figure 3.** FTIR spectra of the series of PORAs obtained from the POHA IP-APAF. Also, the corresponding POHA is depicted.
- Figure 4.** WAXD analysis of acetyl (a) and pivaloyl (b) APAF PORAs.
- Figure 5.** Free volume fraction as a function of intersegmental distance.
- Figure 6.** TGA analysis for the acetyl (a) and pivaloyl (b) DPS-APAF PORAs.
- Figure 7.** Stress-strain curves for IP-APAF- Ac and IP-APAF-Pv polymers.
- Figure 8.** Robeson plot for He/N₂ (a) and He/CH₄ (b) for all the APAF PORAs studied. Black symbols correspond to the acetyl PORAs while white signs correspond to the pivaloyl ones.
- Figure 9.** Robeson plot for He/CO₂ for all the APAF PORAs studied. Black symbols correspond to the acetyl PORAs while white symbols correspond to the pivaloyl ones.
- Figure 10.** Permeability to all the gases studied as a function of 1/FFV.
- Figure 11.** Permeability to He and CO₂ (a) and He/CO₂ selectivity (b) as a function of the intersegmental distance (d-spacing). Stars in (a) correspond to the molecular size of He and CO₂. The hard sphere size of H₂ is also marked as a vertical dash.

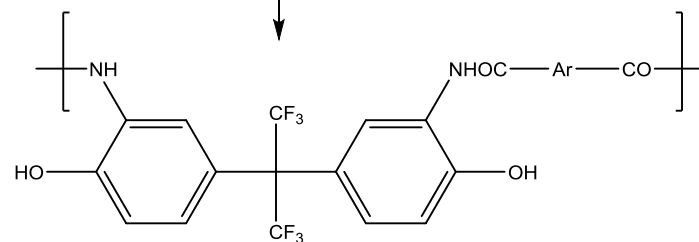
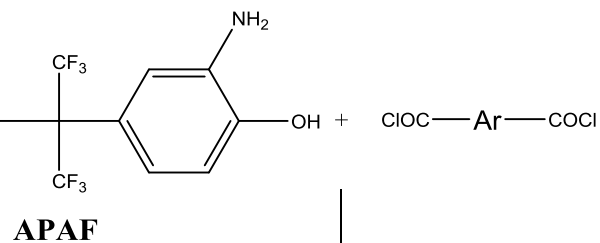


$\text{R} = \text{C}(\text{CF}_3)_2$ **6FC**

$\text{R} = \text{SO}_2$ **DPSC**

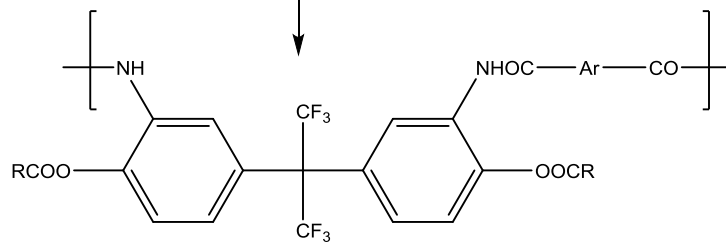
ACS Paragon Plus Environment

Figure 1. Scheme of the synthesis of the dichlorides from diacids.

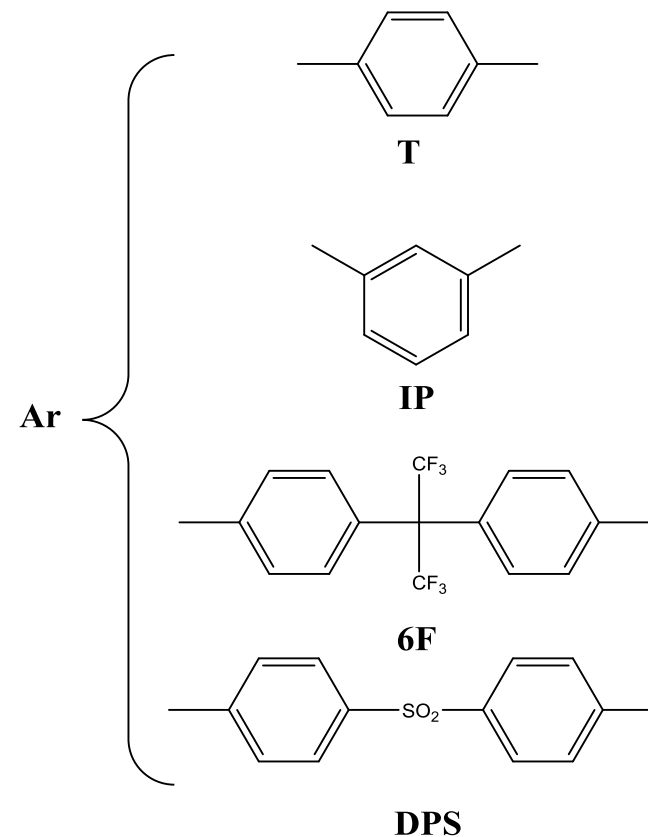


POHA [Ar-APAF]

RCOCl or (RCO)₂O / Py



**PORA [R= CH₃; Ar-APAF-Ac]
[R= C(CH₃)₃; Ar-APAF-Piv]**



1
2
3
4
5
6
7
8
9
10
11
12
13
14
15
16
17
18
19
20
21
22
23
24
25
26
27
28
29
30
31
32
33
34
35
36
37
38
39
40
41
42

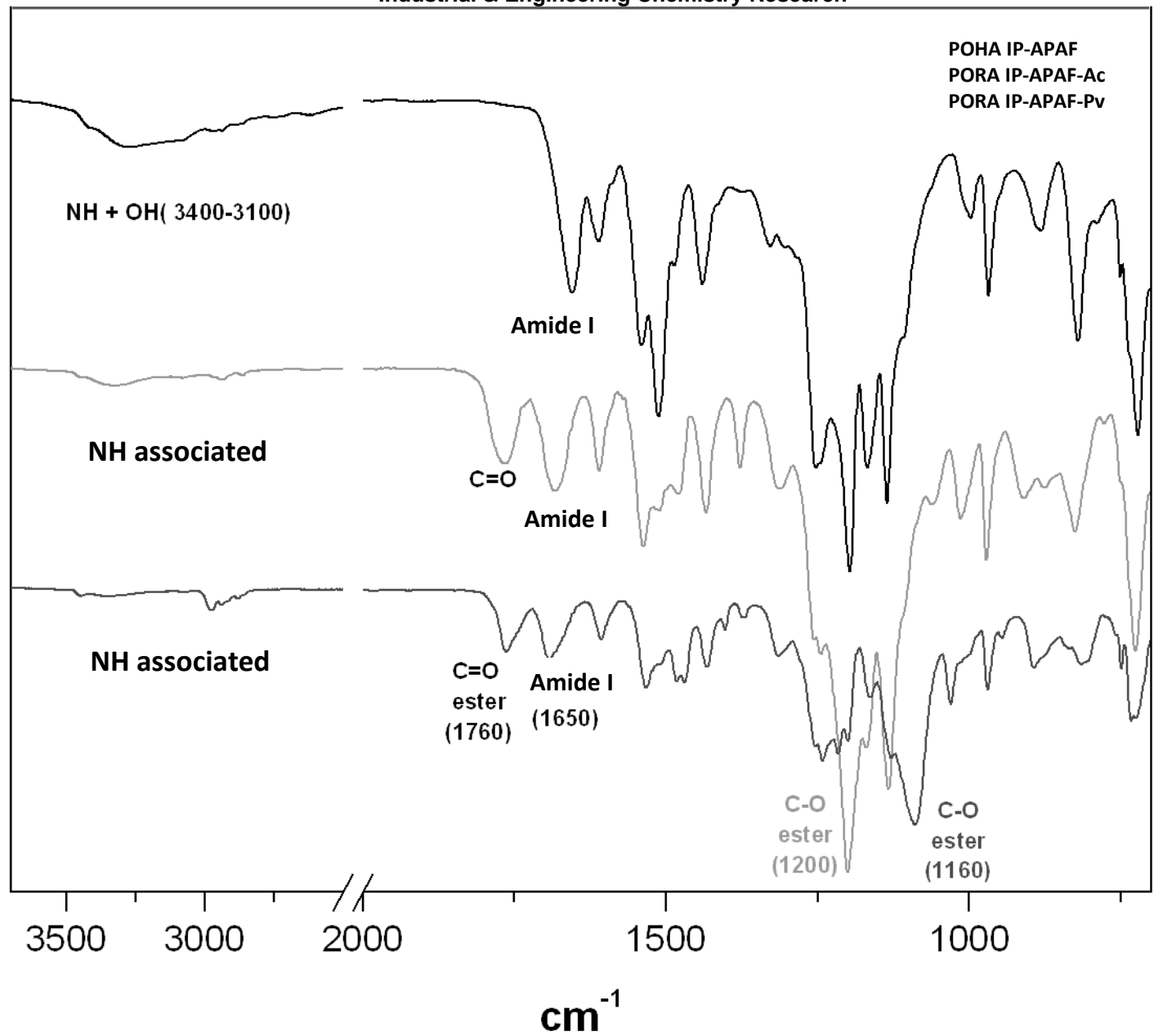
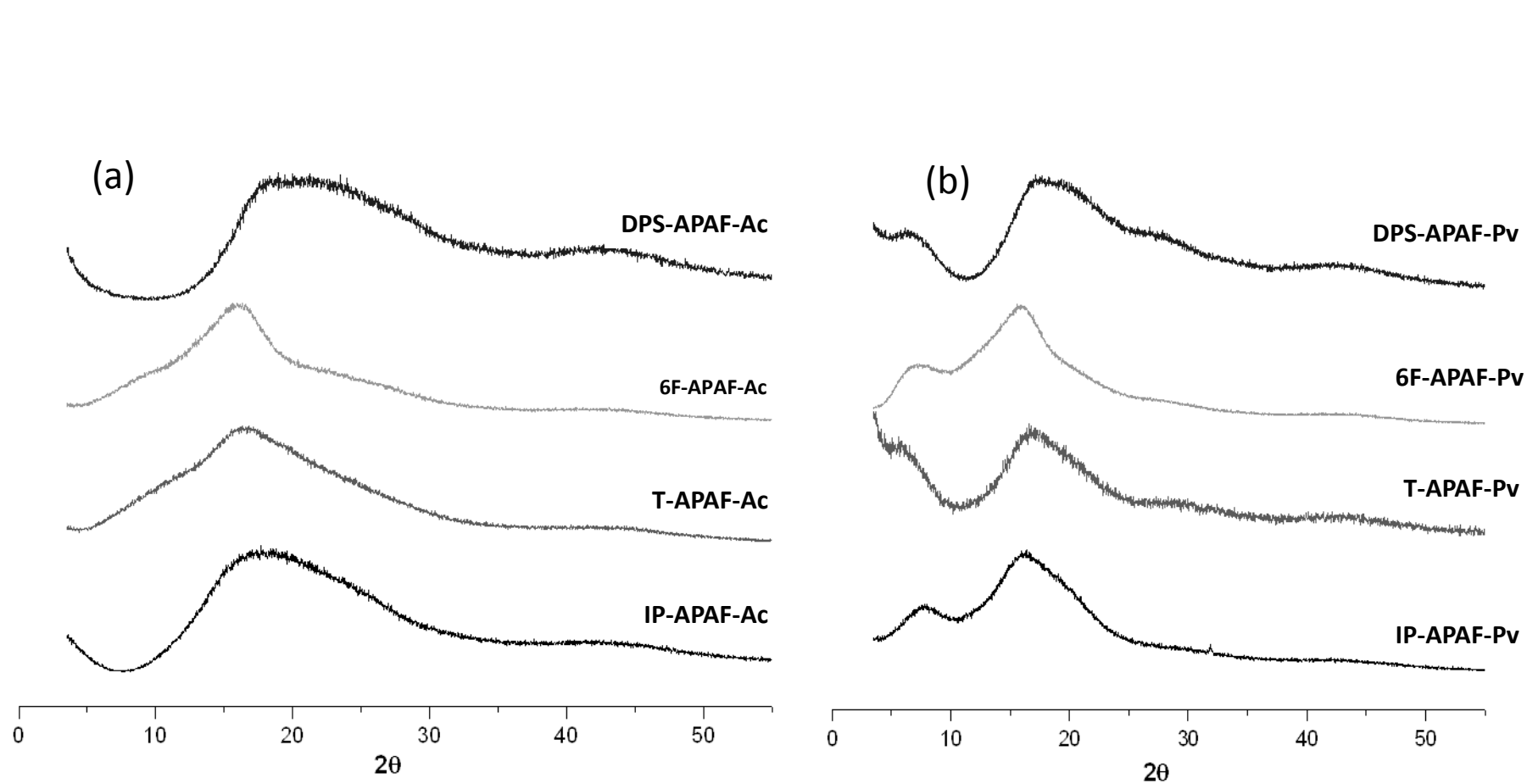
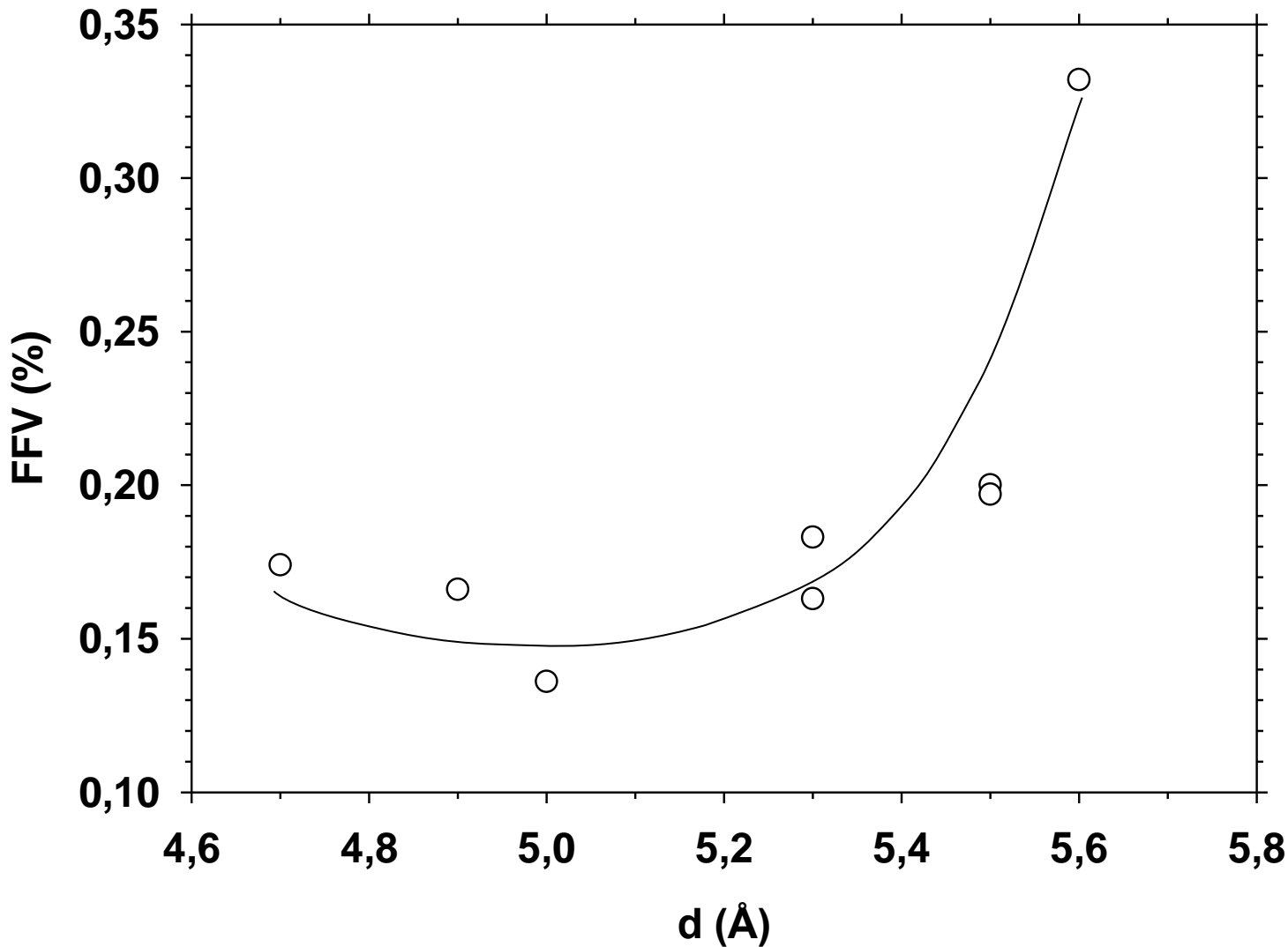


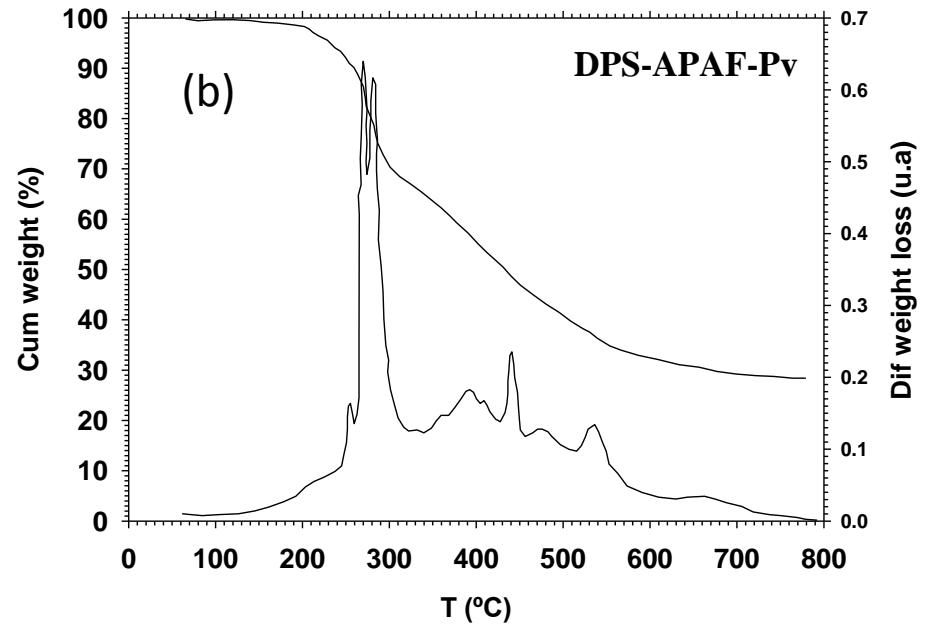
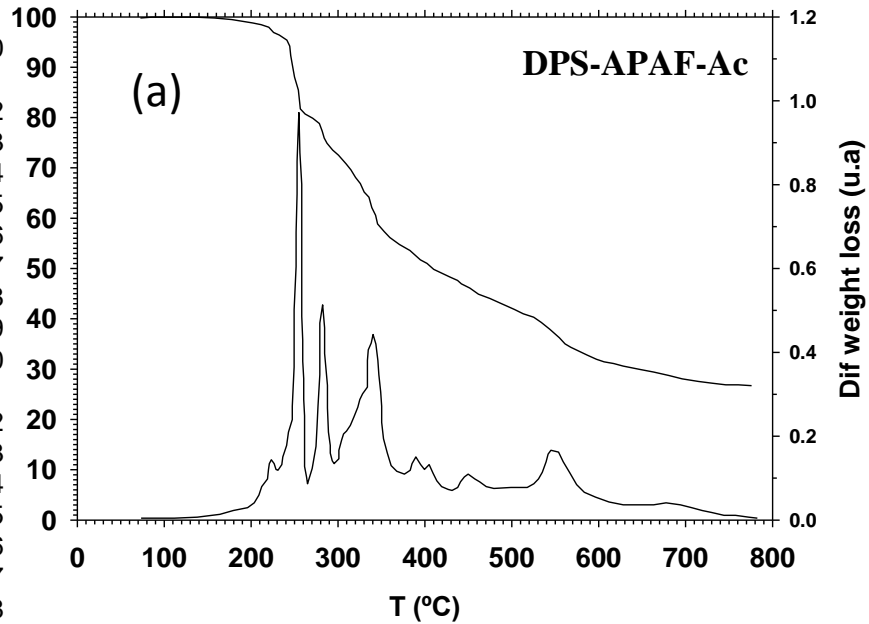
Figure 3. FTIR spectra of the series of PORAs obtained from the POHA IP-APAF. Also, the corresponding POHA is depicted.

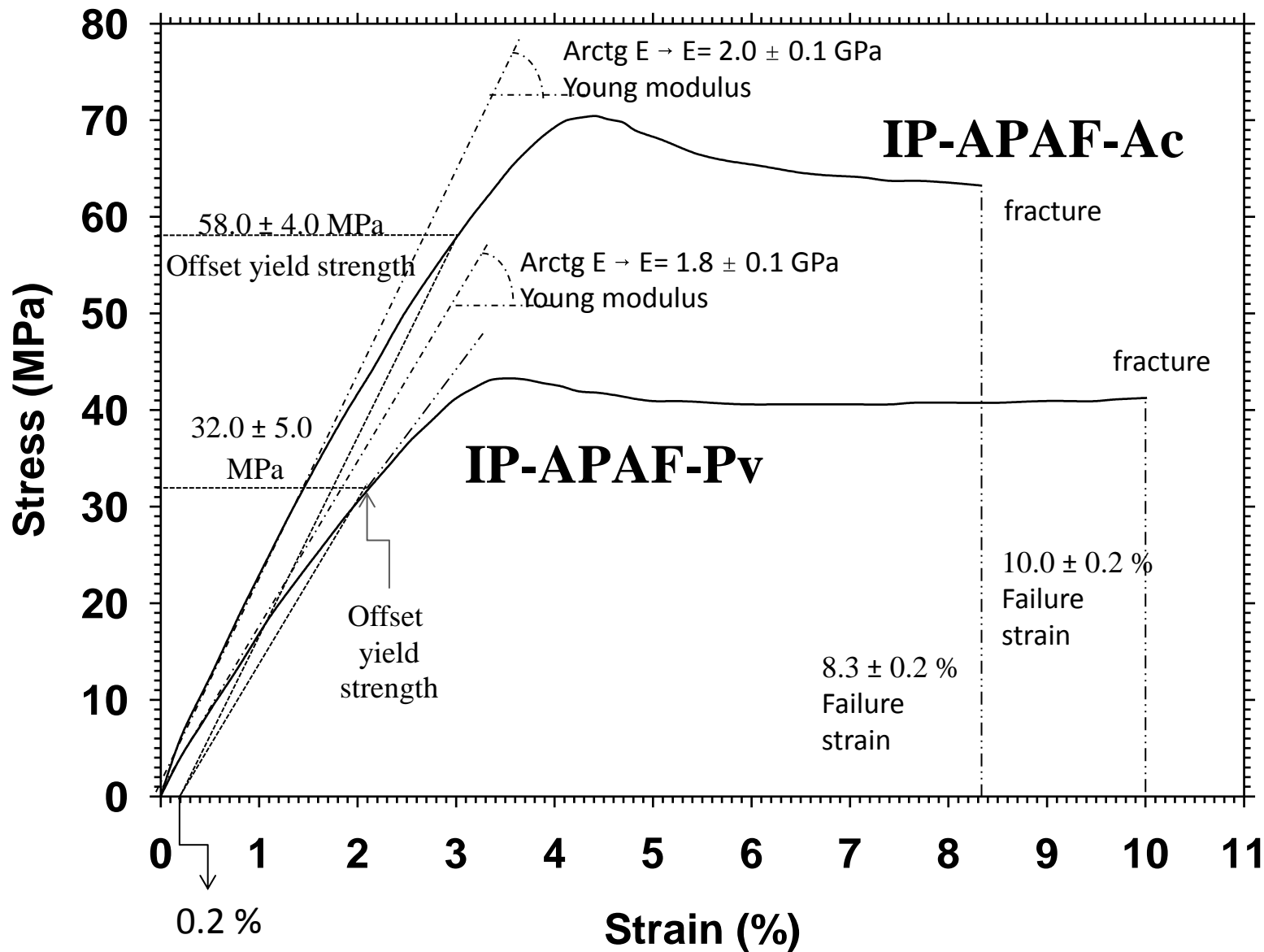




ACS Paragon Plus Environment

Figure 5. Free volume fraction as a function of intersegmental distance.

1
2
3
4
5
6
7
8
9
10
11
12
13
14
15
16
17
18
19
20
21
22
23
24
25
26
27
28
29
30
31
32
33
34
35
36
37
38
39
40
41
42



ACS Paragon Plus Environment

Figure 7. Stress-strain curves for IP-APAF-Ac and IP-APAF-Pv polymers.

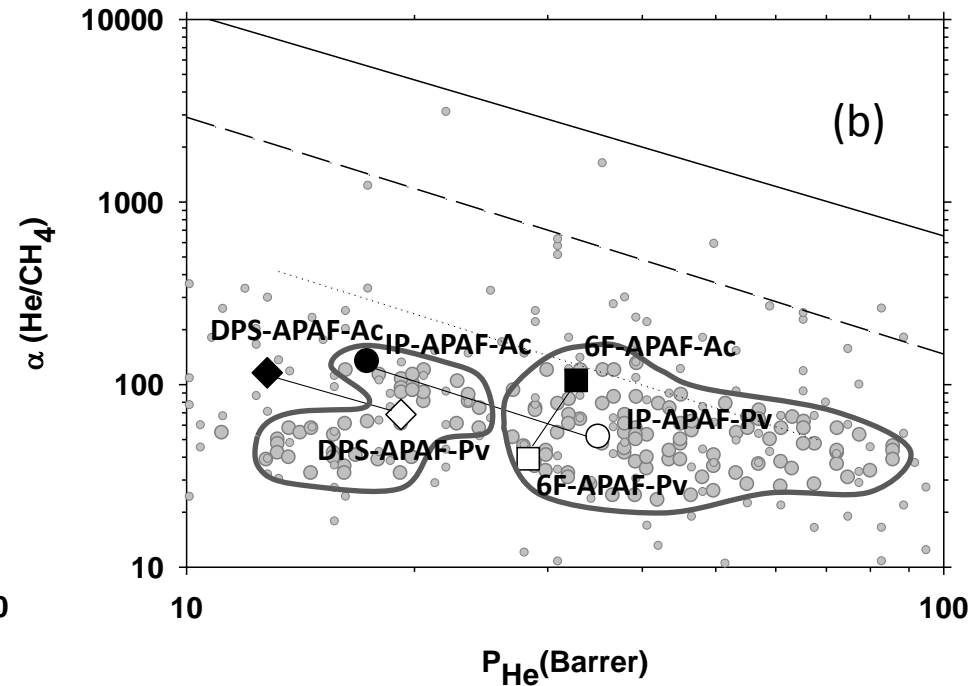
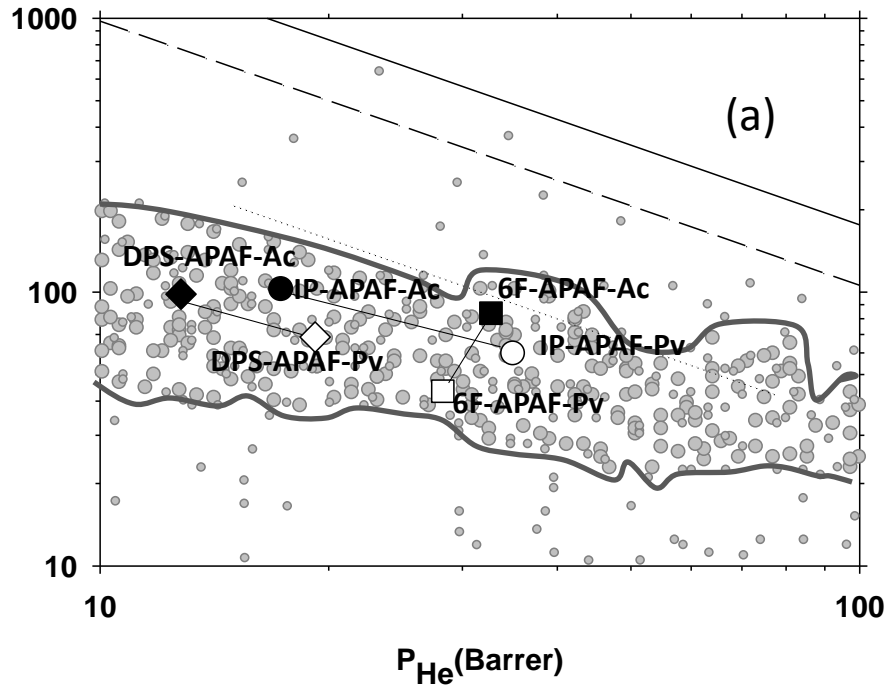
1
2
3
4
5
6
7
8
9
10
11
12
13
14
15
16
17
18
19
20
21
22
23
24
25
26
27
28
29
30
31
32
33
34
35
36
37
38
39
40
41
42

Figure 8. Robeson plot for He/N₂ (a) and He/CH₄ (b) for all the APAF PORAs studied. Black symbols correspond to the acetyl PORAs while white signs correspond to the pivaloyl ones.

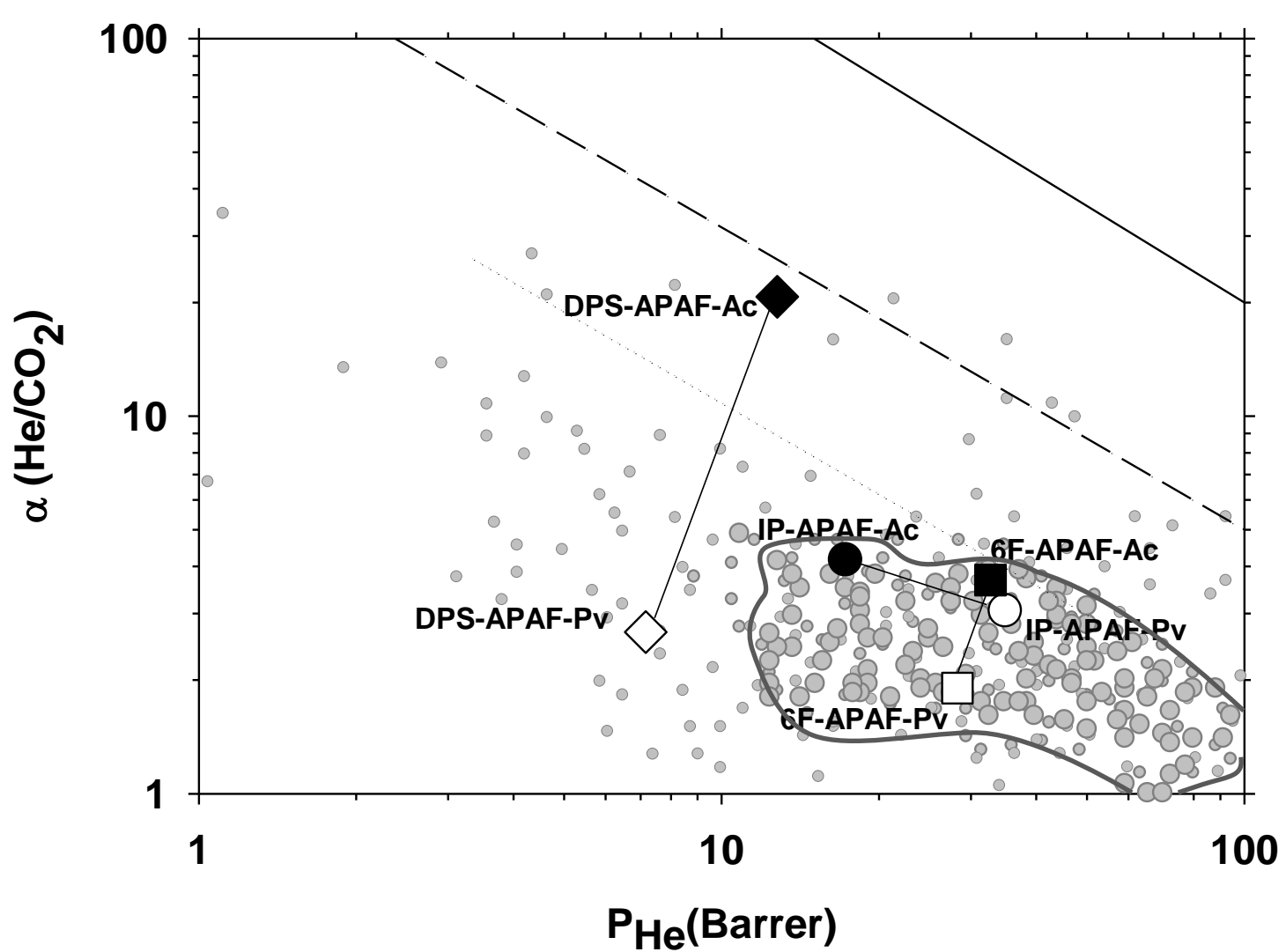
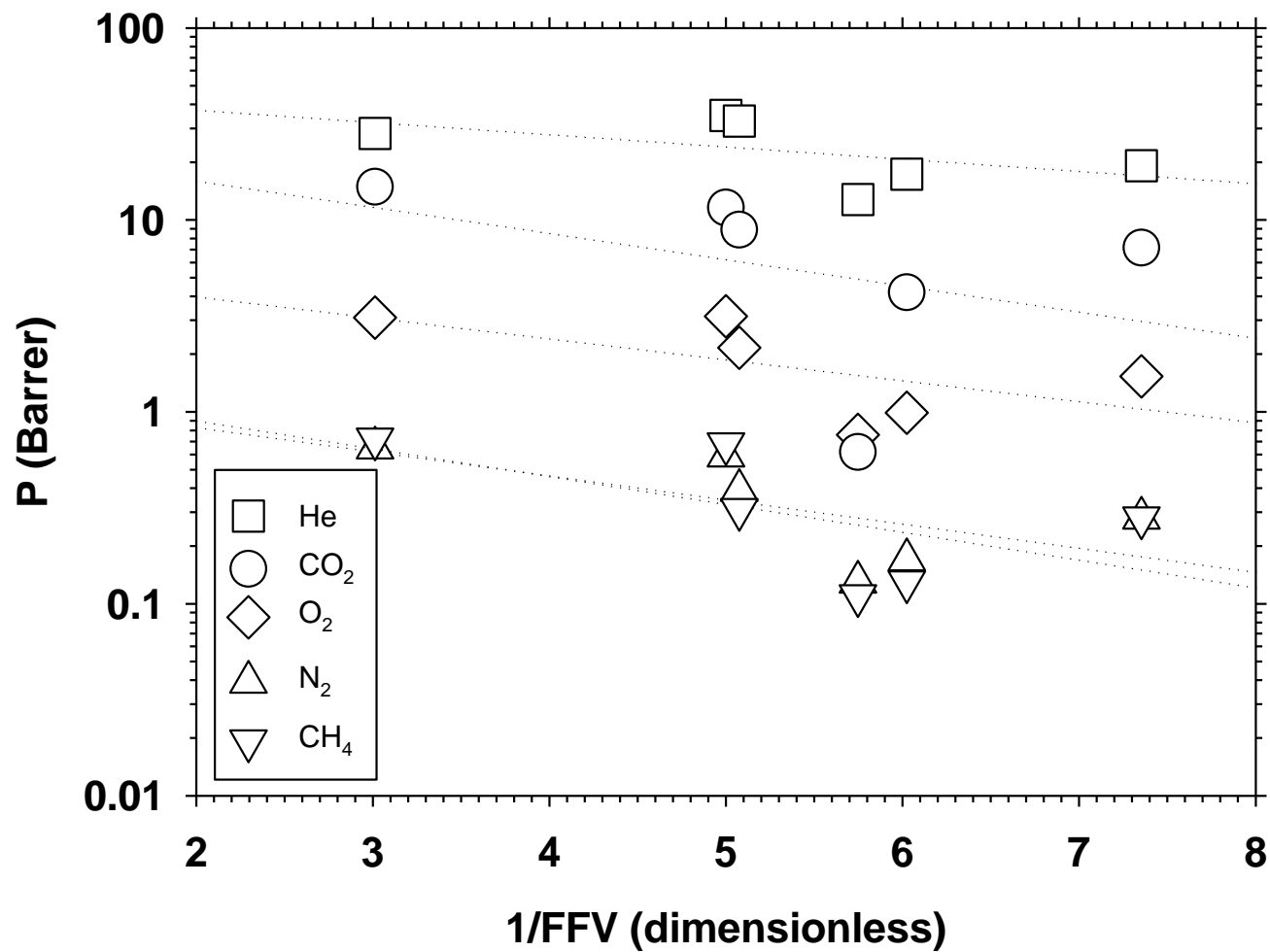


Figure 9. Robeson plot for He/CO₂ for all the APAF-PORAS studied. Black symbols correspond to the acetyl PORAS while white symbols correspond to the pivaloyl ones.

1
2
3
4
5
6
7
8
9
10
11
12
13
14
15
16
17
18
19
20
21
22
23
24
25
26
27
28
29
30
31
32
33
34
35
36
37
38
39
40
41
42



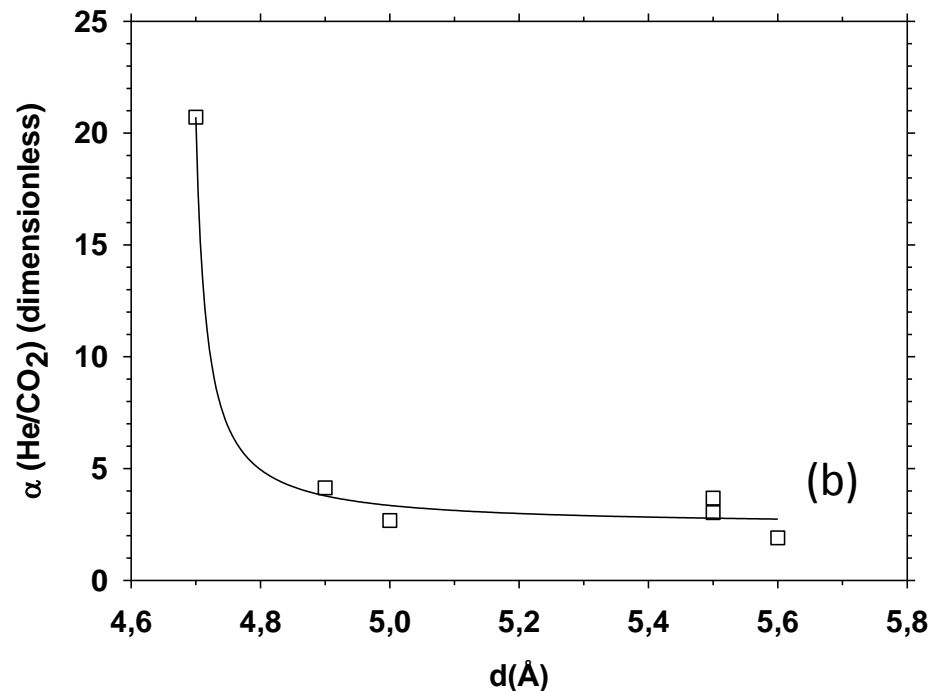
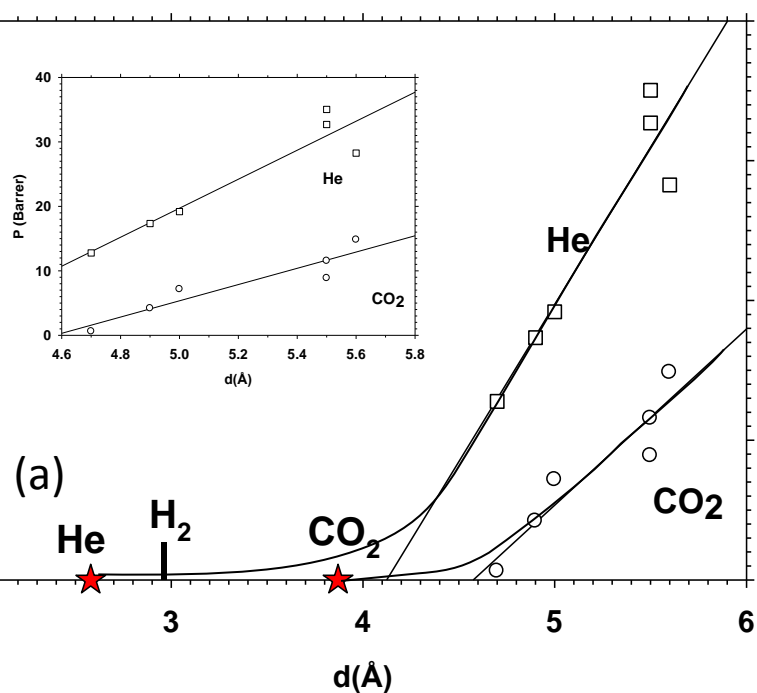
1
2
3
4
5
6
7
8
9
10
11
12
13
14
15
16
17
18
19
20
21
22
23
24
25
26
27
28
29
30
31
32
33
34
35
36
37
38
39
40
41
42

Figure 11. Permeability to He and CO₂ (a) and He/CO₂ selectivity (b) as a function of the intersegmental distance (*d*-spacing). Stars in (a) correspond to the molecular size of He and CO₂. The hard sphere size of H₂ is also marked as a vertical dash.